molecules

MDPI

Article

Photoelectrocatalytic Processes of TiO_2 Film: The Dominating Factors for the Degradation of Methyl Orange and the Understanding of Mechanism

Yuhui Xiong [1,†], Sijie Ma [2,†], Xiaodong Hong [2], Jiapeng Long [1,*] and Guangjin Wang [2,*]

[1] School of Materials Science and Engineering, Shenyang University of Chemical Technology, Shenyang 110142, China; 2013020230@stu.syuct.edu.cn
[2] School of Materials Science and Hydrogen Energy, Foshan University, Foshan 528051, China; 15729508936@163.com (S.M.); hongxiaodong@lntu.edu.cn (X.H.)
* Correspondence: long2682@126.com (J.L.); wgj501@163.com (G.W.)
† These authors contributed equally to this work.

Abstract: Various thicknesses of TiO_2 films were prepared by the sol–gel method and spin-coating process. These prepared TiO_2 films exhibit thickness-dependent photoelectrochemical performance. The 1.09-µm-thickTiO_2 film with 20 spin-coating layers (TiO_2-20) exhibits the highest short circuit current of 0.21 $mAcm^{-2}$ and open circuit voltage of 0.58 V among all samples and exhibits a low PEC reaction energy barrier and fast kinetic process. Photoelectrocatalytic (PEC) degradation of methyl orange (MO) by TiO_2 films was carried out under UV light. The roles of bias, film thickness, pH value, and ion properties were systematically studied because they are the four most important factors dominating the PEC performance of TiO_2 films. The optimized values of bias, film thickness, and pH are 1.0 V, 1.09 µm, and 12, respectively, which were obtained according to the data of the PEC degradation of MO. The effect of ion properties on the PEC efficiency of TiO_2-20 was also analyzed by using halide as targeted ions. The "activated" halide ions significantly promoted the PEC efficiency and the order was determined as Br > Cl > F. The PEC efficiency increased with increasing Cl content, up until the optimized value of 30×10^{-3} M. Finally, a complete degradation of MO by TiO_2-20 was achieved in 1.5 h, with total optimization of the four factors: 1.0 V bias, 1.09-µm-thick, pH 12, and 30×10^{-3} M Cl ion content. The roles of reactive oxygen species and electric charge of photoelectrodes were also explored based on photoelectrochemical characterizations and membrane-separated reactors. Hydrogen peroxide, superoxide radical, and hydroxyl radical were found responsible for the decolorization of MO.

Keywords: TiO_2; photoelectrochemical performance; photoelectrocatalytic performance; methyl orange; reactive oxygen species

Citation: Xiong, Y.; Ma, S.; Hong, X.; Long, J.; Wang, G. Photoelectrocatalytic Processes of TiO_2 Film: The Dominating Factors for the Degradation of Methyl Orange and the Understanding of Mechanism. *Molecules* **2023**, *28*, 7967. https://doi.org/10.3390/molecules28247967

Academic Editor: Łukasz Chrzanowski

Received: 3 November 2023
Revised: 22 November 2023
Accepted: 1 December 2023
Published: 6 December 2023

1. Introduction

Energy and environmental crises have become serious threats to human society in the world today. Industrialization and population growth are major factors that result in environmental pollution and energy shortages [1]. Organic materials including dyes dumped into the water by organic industries are hazardous to aquatic life. The production of synthetic dyes has increased rapidly to meet the demands of the textile, food, printing, ink, tannery, paper, pharmaceutical, and cosmetic industries. However, the chemicals used in the production of these dyes are toxic and carcinogenic [2]. Therefore, it is obligatory for the scientific community to explore ways for overcoming the issues related to industrial effluents loaded with dye contaminants [3].

Photoelectrocatalysis (PECs) has attracted considerable interest since the discovery of the Honda–Fujishima effect [4] in 1972, especially following the serial stories reported by Carey et al. [5,6] that degradation-resistant organics such as polychlorinated biphenyl can

be decomposed by TiO_2 photoelectrode. In 1989, Tanaka, K. et al. [7] proved that reactive oxygen species (ROSs) such as hydroxyl radicals (•OH) play a key role in photocatalysis, achieving great progress in photocatalytic (PC) mechanism. Furthermore, ROSs can be more effectively produced in photoelectrocatalytic (PEC) processes in a voltage bias photoelectrode, contributing significantly to the PEC synergy effect and enhanced PEC efficiency [8,9]. PECs combines the advantages of both PC and electrocatalytic technologies. Palanisamy's group [10] demonstrated that the PEC process effectively eliminated 76.2% of amoxicillin within 120 min at 0.8 V, outperforming the removal rates attained by the PC (52.6%) and electrocatalytic (32.3%) processes. PECs can both make use of the solar energy and regulate the photocatalytic process by using photoelectrodes with an appropriate external bias. Moreover, the PEC process is convenient for recycling photoelectrodes, avoiding the dilemma encountered in the photocatalytic process. PECs have been regarded as a technique revolution owing to the combination of photocatalysis, electrocatalysis, and solar energy utilization [11].

Various factors affecting PEC performance have been widely reported for TiO_2 photoelectrodes. Zhao's group [12] observed that anatase TiO_2 with a {001} crystal plane exposed shows prominent PEC activity. Wang and co-authors [13] demonstrated that the PEC efficiency increases when the UV light intensity ranges from 700 μWcm^{-2} to 2.5 $mWcm^{-2}$. Iltaf Shah et al. [2] revealed that a basic alkaline medium is more suitable for a higher degradation rate of ethyl violet dye than acidic and neutral media. Lu Li and his teammates [14] announced that the PEC kinetics constant (K') was a 6.0-fold increase compared to the PC system. They observed that the PEC degradation efficiency of o-chlorophenol was 96.6% in 180 min under optimum conditions (bias: 0.5 V, solution pH: 6.3). Yan et al. [15] claimed that the PEC efficiency is approximately proportional to the thickness of the TiO_2 film; however, excessive thickness causes deterioration of the PEC efficiency. Anderson's team [16] reported the effect of bias, pH, inorganic ions on the PEC efficiency. Particularly, halide ions can be "activated" by a photoelectrode with sufficient bias and transformed into an "active halide" with highly catalytic oxidation activity, greatly improving the PEC efficiency of decomposing seawater to produce hydrogen [17]. To conclude, extensive investigations have been carried out on one or several of the factors affecting the PEC efficiency of TiO_2, including the crystal phase, light source and light intensity, film thickness, bias, ion properties, and pH value [11]. However, a systematic study on the factors dominating the PEC efficiency and related mechanisms is still absent so far.

Numerous metal oxides such as TiO_2, SnO_2, ZnO, WO_3, and Cu_2O have been used as photoelectrodes in PECs [18]. TiO_2 is considered one of the most important photoelectrodes due to its high activity, stability, and low cost [19]. Various forms of nanostructured TiO_2 film have been used in various applications such as detectors, memories, high-efficiency hydrolysis, diodes, transistors, sensors, etc. [20,21]. With regard to the feasibility of the application of TiO_2 photoelectrodes, film thickness, bias, ion properties, and pH value are the four most important factors. Therefore, in this study, we initiate a systematic study on the four factors dominating the PEC efficiency. The roles of ROSs and the electric charge of electrodes were also investigated to explore the related PEC mechanisms based on photoelectrochemical characterizations combined with membrane-separated reactors. This study might be beneficial to PEC research fields involved in the appropriate choice and optimization of experimental conditions and parameters.

2. Results

2.1. Structure, Morphology, and Optimal Properties of TiO_2 Films

Figure 1a shows the X ray diffraction (XRD) pattern of TiO_2-20. All the diffraction peaks in the pattern are well-indexed to TiO_2 and F-doped tin oxide (FTO). The peaks located at 2θ = 25.3°, 37.8°, 39.2°, 48.1°, 55.1°, 56.2°, and 69.1° are attributed to anatase types of TiO_2. No other diffraction peak arises from possible impurities, indicating that a pure-phase TiO_2 film is produced. The variation curves of thickness and absorbance of the

films are given as the number of layers in Figure 1b. It is obvious that both the thickness and absorbance of the films increase with increasing layers of coatings.

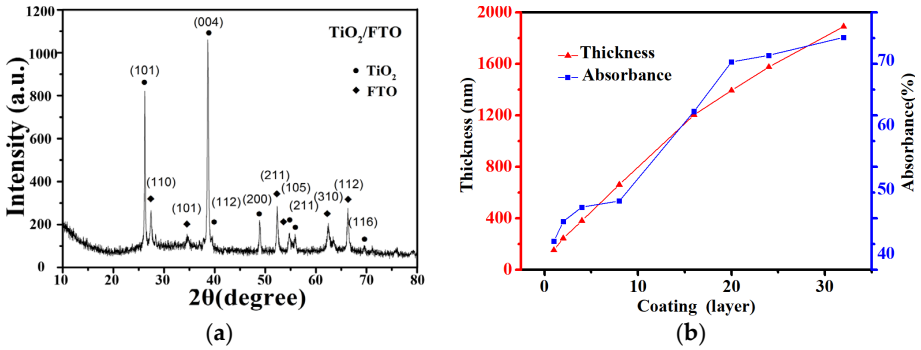

Figure 1. (**a**) XRD pattern of TiO_2-20, (**b**) the variation curves of film thickness and absorbance as the layers of coatings increase.

Figure 2a–c shows the scanning electron microscopy (SEM) images of TiO_2-1, TiO_2-4, and TiO_2-20. TiO_2-1 has a uniform, smooth, and dense surface (Figure 2c). We observed that the surface morphologies of TiO_2-2 and -3 are similar to that of TiO_2-1. Cracks began to appear in TiO_2-4 and then gradually widened as the layers increased. SEM images of TiO_2-4 and -20 in Figure 2b,c are given, respectively, as representative examples. The inset in Figure 2a is the high-magnification SEM image of TiO_2-1. The surface morphology in the red box in Figure 2b,c is similar to that of the inset. The results indicate that all TiO_2 films are composed of nanoparticles with a size of 20–30 nm. The microstructure of the TiO_2 films was further investigated with transmission electron microscopy (TEM). Figure 2d shows the representative TEM images of TiO_2-20. Grain crystal particles of TiO_2-20 shown in the TEM image can be clearly observed, which also indicate that TiO_2-20 is composed of 20–30 nm size nanoparticles.

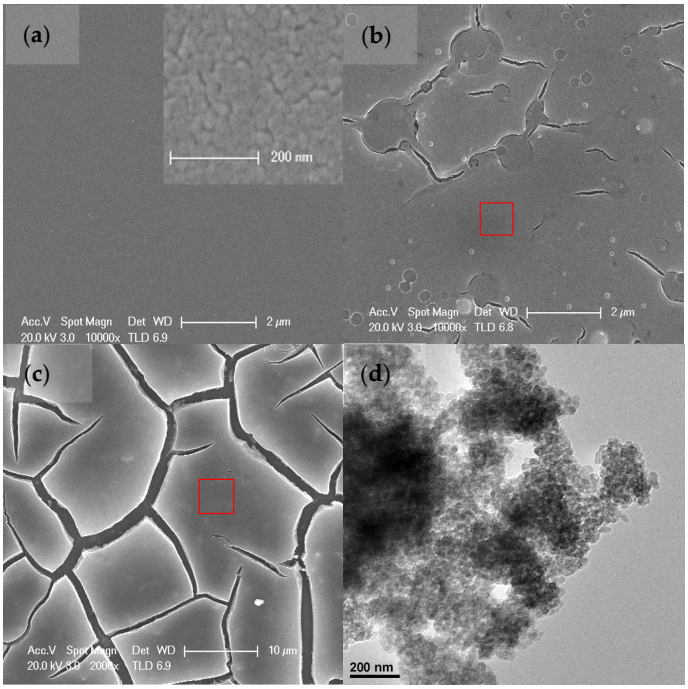

Figure 2. (**a**) SEM images of TiO_2-1, (**b**) TiO_2-4, (**c**) TiO_2-20, and (**d**) TEM of TiO_2-20. Inset is the close-ups of TiO_2-1. Red boxes in Figure 2b,c designate two continuous small areas in surface of TiO_2-4 and TiO_2-20.

2.2. Photoelectrochemical Properties of TiO_2 Photoelectrodes

Before the measurement of PEC regulation of MO by TiO_2 photoelectrodes, the cyclic voltammetry (CV) technique was used to examine the charge transfer between the FTO and the electrolyte. Figure 3a shows that the onset potentials for the anodic and cathodic dark current are essentially independent of the film thickness and scan rate. Representative samples of TiO_2-1, -8, -20, and -32 displayed nearly perfect blocking characteristics, indicating that all the films are pinhole free [22]. The result is also supported by the SEM data showing that the surface of the FTO substrate is completely covered by a very thin and compact TiO_2 coating. Moreover, even if there are cracks in some of the TiO_2 samples such as TiO_2-20, the inner coatings contacting the FTO substrates are still uniform and dense enough to separate FTO substrates from electrolytes, blocking charge transfer between them. In this case, charge transfer can only proceed between the TiO_2 photoelectrode and the electrolyte in the PEC reaction. The position of the flat-band potential was obtained by taking the x intercept of the Mott–Schottky plots of the TiO_2 films (Figure 3b), which gave all the samples a considerably negative flat-band potential, for example, −0.51 V for TiO_2-20. The positive slope of the plots again proved the n-type nature of the TiO_2 films. The application of a potential over the flat-band potential can suppress the charge carrier recombination. Thus, a zero or positive bias over the flat-band potential on the TiO_2 film electrodes may improve the PEC efficiency.

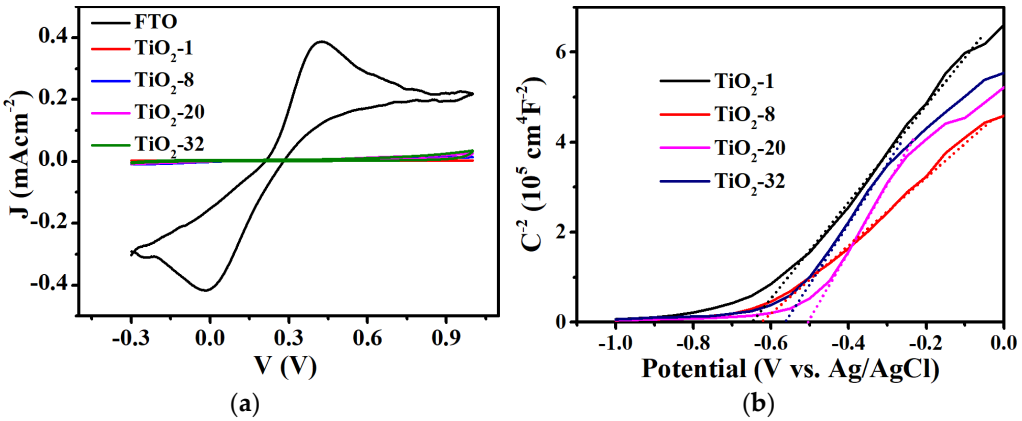

Figure 3. (**a**) CV of FTO, TiO_2-1, -8, -20, and -32. The measurement was carried out by a three-electrode system with TiO_2 film as working electrode, Pt plate as counter electrode, and Ag/AgCl electrode as reference electrode, respectively, and a scan rate of 20 mV s^{-1}. The electrolyte solution was 0.5×10^{-3} M $K_4Fe(CN)_6$ + 0.5×10^{-3} M $K_3Fe(CN)_6$ in aqueous 0.5 M KCl. (**b**) Mott–Schottky plots of TiO_2 films; measured at 10 kHz, sweep rate 100 mVs^{-1}. The electrolyte solution was 0.5×10^{-3} M Na_2SO_4.

Figure 4a,b shows the variation in the short circuit current (I_{SC}) and open circuit voltage (V_{OC}) as the layers of TiO_2 coatings. The data of I_{SC}, V_{OC}, and film thickness were abstracted from Figure S3. The behavior of the anode photocurrent and shift to negative potential under irradiation in Figure S3 indicate an n-type semiconductor behavior. The I_{SC} and V_{OC} increased at first and then decreased as the film thickness increased. TiO_2-20 achieved the highest I_{SC} of 0.21 $mAcm^{-2}$ and V_{OC} of 0.58 V. The thickness-dependent photoelectrochemical properties of the TiO_2 films were also observed by M. L. Hitchman [23] and M. Rodríguez-Pérez [24] in polycrystalline anatase. EIS is particularly useful for explaining the interface charge transport and recombination [25]. Figure 4c shows Nyquist plots of the TiO_2-1, -8, -16, -20, -24, -32. The zoom of the high-frequency range in Figure 4d indicates that the semicircle part of TiO_2-20 has a minimum diameter among all the TiO_2 films. In the same frequency, a small impedance semicircle indicates a large capacitance value at the corresponding time constant and a low Faraday current impedance, signifying a fast kinetic process [26]. Thus, TiO_2-20 was chosen and used for the follow-up PEC experiment owing to its fast kinetic process and low PEC reaction energy barrier.

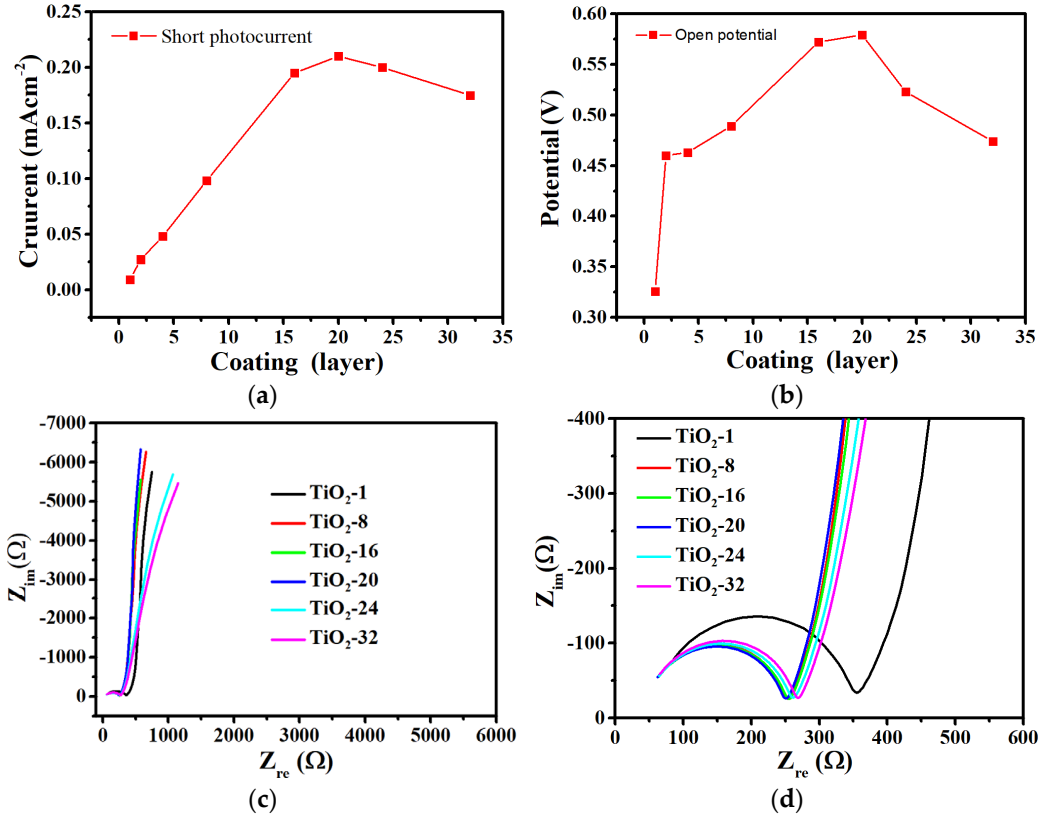

Figure 4. Patterns of variation in (**a**) short circuit current and (**b**) open circuit voltage as the layers of coatings of TiO_2 films. (**c**) Complete range Nyquist plot and (**d**) zoom at high-frequency region. Measuring condition: a 20 mV of AC signal was applied for a frequency range from 100 mHz to 400 kHz under UV-LED irradiation at a direct current bias of 0 V. The electrolyte solution was 0.5×10^{-3} M Na_2SO_4.

2.3. PEC Degradation of MO by TiO_2 Photoelectrodes

We carried out the PEC degradation of MO using the PEC reactor as shown in Scheme 1a. Figure 5a shows the variation in the degradation rate of pristine MO using the TiO_2-20 photoelectrode, with the potential bias ranging from 0 V to 1.2 V. Generally, in the PEC process, the degradation rate increased with an increasing bias, up until the optimized value of 1.0 V. Song et al. [27] and Zanoni et al. [28] reported similar results, in which at the optimal potential bias (for a given light intensity and film thickness), the electrons and holes were so well separated that enhancing the potential bias led to no significant improvement in the PEC activity. The PEC degradation of MO was further carried out using different thicknesses of TiO_2 photoelectrodes. As expected, TiO_2-20 achieved the highest degradation rate of 88.6% in 6 h among the representative samples at a bias of 1.0 V (Figure S4). This result is in accordance with the data of photoelectrochemical characterizations. Therefore, PEC regulation of MO by TiO_2-20 with a 1.0 V bias was chosen and used for the tests of different pH, halide ion, and concentrations of Cl, respectively.

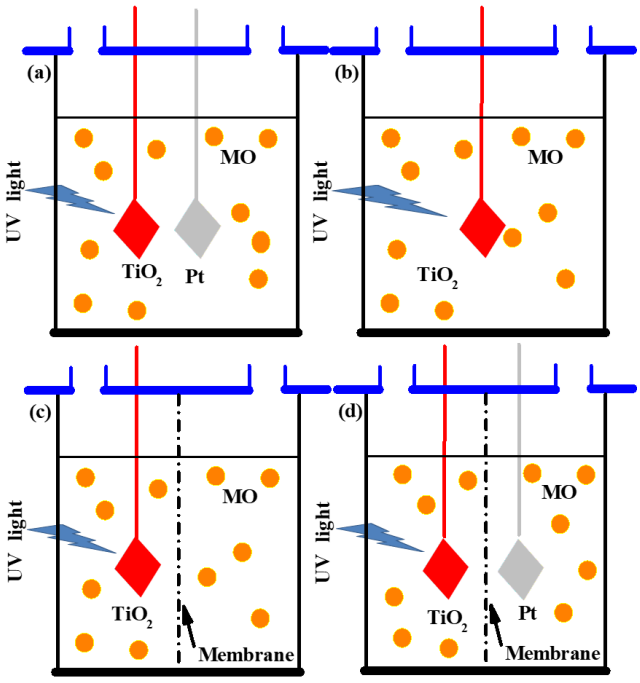

Scheme 1. Schematic diagrams of experimental reactors with about 100 mL of volume glass container for PEC and PC regulation of MO. (**a**) PEC, (**b**) PC, (**c**) PEMS, and (**d**) PECMS reactors.

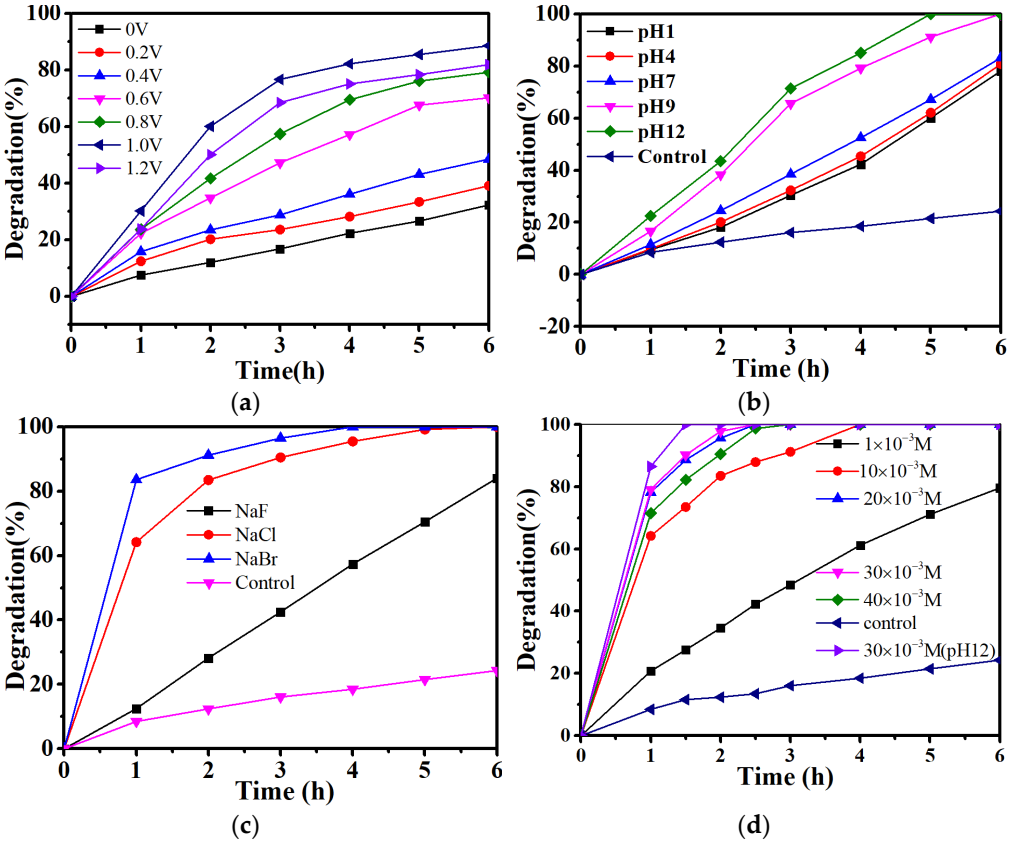

Figure 5. (**a**) PEC regulation of original MO by TiO_2-20 at different bias. PEC regulation of MO by TiO_2-20 with 1.0 V bias at different (**b**) pH, (**c**) halide ions, and (**d**) concentrations of Cl. The PEC reactor is depicted as Scheme 1a.

Figure 5b shows the degradation rates of MO by TiO_2-20 with 1.0 V bias at different pH levels of 1, 4, 7, 9, and 12. The pH value of the solution was adjusted by dropwise adding H_2SO_4 and NaOH. The pH value of original MO solution in the control experiment was 5.8. One can see that the increasing pH value contributes to an enhanced degradation rate. Moreover, the degradation rates of all pH-adjusted MO solutions are higher than that of the pristine one. The reason is that the high conductivity of the MO solution increases the mass transfer and improves the PEC efficiency due to the addition of electrolytes H_2SO_4 and/or NaOH [29].

The influence of different electrolytes on the PEC degradation of organics has extensively been investigated in NaCl, $NaNO_3$ and Na_2SO_4, NaBr, and $NaClO_4$ [15,29,30]. The effects depend on the types and concentrations of negatively charged ions [11]. Halide ions can be transformed into "active halide" with highly catalytic oxidation activity, substantially improving the PEC efficiency and producing organic halides of industrial and medicinal importance [17]. Thus, in this study, we focused on the effect of halide ions on the PEC efficiency of TiO_2-20. Iodine ion (I^-) was not included here because of its highly chemical reduction [31]. Figure 5c shows the degradation of MO by halide ions F, Cl, and Br. The order of the PEC efficiency was determined as Br > Cl > F. The halide ions can be activated to form highly oxidizing free radicals, significantly improving the PEC efficiency [30]. Considering that the Cl ion is very important and spreads over the water on earth, we carried out PEC experiments on the degradation of MO with different concentrations of Cl ion. Figure 5d shows that the addition of Cl greatly increased the photocurrent and PEC efficiency. The degradation rate rapidly increased as the Cl content increased from 0 to 10×10^{-3} M. However, the increase in the degradation rate slowed down as the concentration of Cl ranged from 10×10^{-3} M to 30×10^{-3} M. Moreover, excessive Cl content caused a decrease in degradation rate. The results indicate that the content of "active" Cl reached nearly its maximum, meaning that increasing the content of Cl cannot produce more "active" Cl but suppresses the PEC efficiency. In all, the PEC efficiency can be substantially improved by optimizing factors dominating the PEC performance of TiO_2 films. A complete degradation of MO by TiO_2-20 was achieved in 1.5 h in the PEC process with total optimization of the four factors: a thickness of 1.09 μm, a bias of 1.0 V, a content of 30×10^{-3} M Cl ion, and pH 12. The PEC degradation efficiency of MO by TiO_2-20 is pretty high and typical examples of comparative literature values are included in Table 1.

Table 1. Typical examples for pollutant degradation using PEC systems. (NPs = nanoparticles, NTs = Nanotubes).

Photoelectrode	Target Pollutant	Degradation Rate (%)	Degradation Time (min)	Ref.
TiO_2NPs	MO	100	90	Our work
TiO_2NPs	amoxicillin	76.2	120	[10]
TiO_2 NTs	triclosan	78.7	30	[32]
Ti/TiO_2NTs	Chlortetracycline	74.2	120	[33]
Y-TiO_2	MO	82.8	360	[34]
Double-faced TiO_2	tetracycline	96.4	60	[35]
Au/TiO_2	MO	54	300	[36]

2.4. The Contrast of PEC and PC Degradation of MO

The contrast of the PEC and PC efficiency of TiO_2-20 was carried out using PCMS and PECMS reactors, as shown in Scheme 1c,d. Figure 6a shows that the degradation rate of MO by TiO_2-20 in the PCMS reactor is 41.5% in 6 h in the PC process, while that with a 1.0 bias in the PCEMS reactor is 100% in 5 h in the PEC process. Figure 6b shows that the TiO_2-20 in the PC reactor earned 26.3% degradation of MO, while the same TiO_2-20 with 0 V bias using the PEC reactor gained an enhanced degradation rate of 32.3%. It is expected that the application of a potential (0 V) over the flat-band potential (−0.51 V for TiO_2-20) can suppress the charge carrier recombination and improve the PEC efficiency according to

data of photoelectrochemical characterizations. These results indicate that the PEC process under electrochemical control achieves a much higher degradation rate than the PC one.

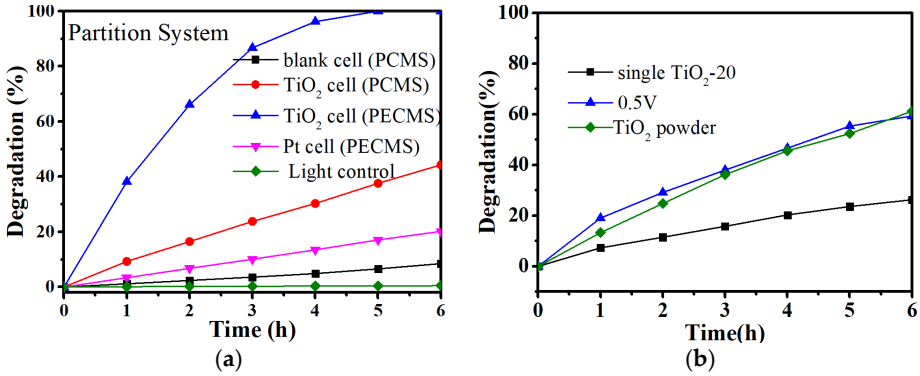

Figure 6. (**a**) The PC and PEC degradation of MO by TiO_2-20 using PCMS (Scheme 1c) and PECMS (Scheme 1d) reactors, respectively. (**b**) The PC degradation of MO by TiO_2 film and powder using PC reactor shown in Scheme 1b.

A comparison of the PEC efficiency of TiO_2-20 in a PEC reactor with the PC efficiency of TiO_2 powder in a PC reactor was also carried out. The film mass of TiO_2-20 was determined as 3.81 mg by measuring the difference of mass between FTO and TiO_2-20-coated FTO. Figure 6b shows that the single TiO_2-20 film can decolor 26.3% of MO, while TiO_2 powder (3.81 mg) can decompose 44.3% of MO in 6 h. The reason is that the TiO_2 powder is highly dispersed and has much larger contact area with MO solution than that of the single TiO_2-20 film. However, the TiO_2 film photoelectrode is very easy to be recycled and reused compared to the TiO_2 powder catalyst. Moreover, the TiO_2 film photoelectrode is convenient for the PEC process. Particularly, the PEC efficiency can be improved by electrochemical regulation; for example, TiO_2-20 with a bias of 0.5 V can achieve an equivalent degradation rate of MO as a 3.81 mg TiO_2 powder (Figure 6b).

2.5. The Roles of ROSs and Electric Charge of Electrodes

The general principle of PECs is well-documented in the pioneering work and follow-up studies [4,37–42]. Scheme 2 shows the energy level diagram of the TiO_2 film and the events possibly occurring during the PEC process. Under UV irradiation, the electrons (e^-) in TiO_2 are excited to the conduction band, which creates holes (h^+) in the valence band. The excited holes can oxidize water into oxygen and interact with O_2 and H_2O to form an assortment of ROSs, (i.e., •OH, H_2O_2). The excited electrons are collected and removed by an external circuit to the counter electrode, where they are frequently captured by oxygen to form ROSs (i.e., $\bullet O_2^-$, H_2O_2). Here, we carried out PC and PEC tests to explore the origin of ROSs with a partition system (see Scheme 1c,d) under different conditions.

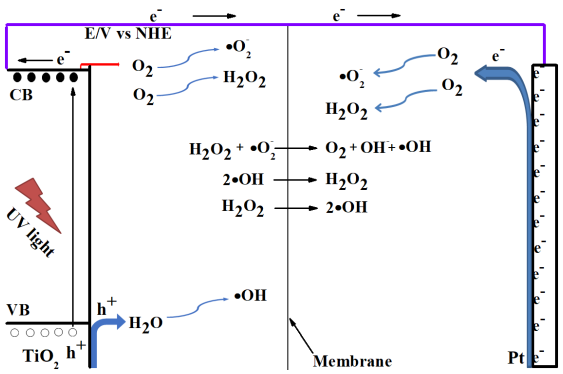

Scheme 2. Energy level diagram of TiO_2 film and the events possibly occurring during the PEC process.

Figure 7a shows that the •OH and$•O_2^-$ yield increased with increased irradiation time in both TiO_2 and Pt cells of the PCEMS reactor (Scheme 1d). The species of •OH in the TiO_2 of the PCEMS reactor were probably produced by a hole-induced oxidation process [43]:

$$H_2O + h^+ \rightarrow •OH + H^+ \quad (1)$$

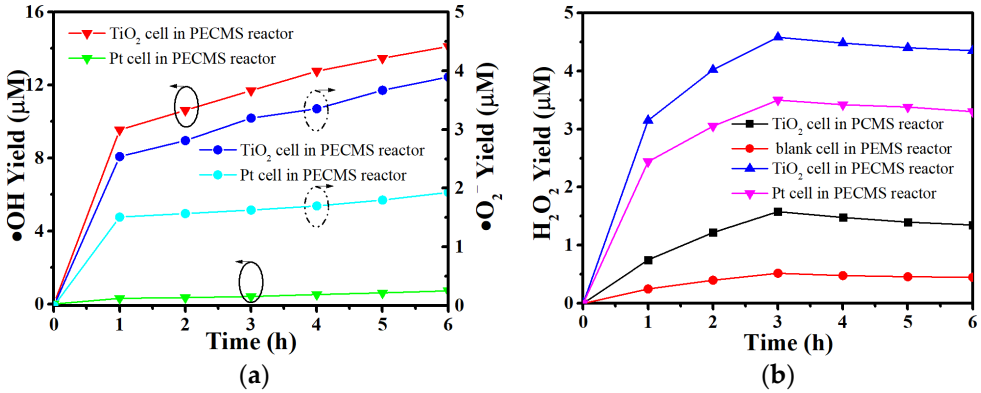

Figure 7. (**a**) •OH, $•O_2^-$, and (**b**) H_2O_2 yield in TiO_2 and Pt cell of PECMS reactor under UV irradiation.

The •OH yield in the Pt cell of the PCEMS reactor should originate from the Pt electrode because •OH in TiO_2 cell has a very short lifetime and cannot pass through the membrane to the Pt cell. It well known that electrons can react with O_2 to produce $•O_2^-$, and then H_2O_2 and •OH through a reductive process (Formulas (2)–(6)) [44,45]. The very low •OH yield suggests that a low level of kinetics evolution of •OH proceeds in the Pt cell of a PCEMS reactor.

$$O_2 + e^- \rightarrow •O_2^- \xrightarrow{2H^+} H_2O_2 \quad (2)$$

$$O_2 + 2H_2O + 2\,e^- \rightarrow H_2O_2 + 2OH^- \quad (3)$$

$$H_2O_2 + •O_2^- \rightarrow •OH + OH^- + O_2 \quad (4)$$

$$2•OH \rightarrow H_2O_2 \quad (5)$$

$$H_2O_2 \xrightarrow{h\upsilon} 2•OH \quad (6)$$

Figure 7b shows that all of the H_2O_2 yields increased at first and became stable with prolonged irradiation time due to the decomposition of H_2O_2 in parallel with its production. The equilibrium concentration of H_2O_2 in the TiO_2 and blank cells of the PEMS reactor was estimated to be 1.48 and 4.8 μM, respectively. It is no doubt that no PC process happened in the blank cell of the PEMS reactor so the supply of H_2O_2 in the blank cell attributed to the diffusion of H_2O_2, which was produced in the PC process of the TiO_2 cell in the PEMS reactor and had a long life span and could pass through the membrane [46].

The equilibrium concentration for H_2O_2 in the TiO_2 and Pt cells of the PECMS reactor significantly increased up to 4.58 and 3.5 μM, respectively. Although H_2O_2 can be derived from •OH according to Formulas (3) and (5), the formation kinetics reaction of H_2O_2 is very slow due to its second-order reaction. In this case, the much higher H_2O_2 yield in the TiO_2 cell compared to the Pt cell of the PECMS reactor suggests that H_2O_2 can be probably produced from other sources. We believe that the supply of H_2O_2 in the TiO_2 cell of the PECMS reactor originates from the back electrons (see the red arrow in Scheme 2) of TiO_2 [47], which were transferred to the solution and underwent a reductive process as

Formulas (2)–(5). The related mechanism and detailed descriptions on back electrons will be published elsewhere.

Note that an 8.5% degradation of MO was observed in 6 h in the blank cell of the PCMS and little degradation of MO under light control indicates that UV light cannot decompose MO in our experimental conditions (Figure 6a). In addition, ROSs including •OH and$\bullet O_2^-$ were produced in the TiO_2 cell of the PCMS, but they cannot pass through the semi-membrane because of their short lifetime. In this case, only H_2O_2 is responsible for the 8.5% degradation of MO in the blank cell of the PCEMS. It is reported that $\bullet O_2^-$ with highly catalytic oxidation activity can also decompose MO [48]. So, H_2O_2, $\bullet O_2^-$, and •OH were responsible for the decolorization of MO. The much higher yields of H_2O_2, $\bullet O_2^-$, and •OH in the TiO_2 cell than those in the Pt cell of the PCEMS reactor suggest that the TiO_2 photoelectrode plays a major role in the PEC process.

3. Materials and Methods

3.1. Materials

Tetrabutyl titanate (99% purity), sodium sulfate (99.0% purity), absolute ethanol (99.9% purity), sodium fluoride, sodium chloride, sodium bromide, MO, sulfuric acid, sodium hydroxyl, and nitric acid were purchased from Sinopharm Group (Shanghai, China). 2,3-bis(2-methoxy-4-nitro-5-sulfophehyl)-2H-tetrazolium-5-carboxanilide (XTT) (>98% purity), Terephthalic acid (TA) (98% purity), and horseradish peroxidase (POD) (activity: 250–330 units/mg solid) were received from Sigma-Aldrich (Shanghai, China). FTO glass was obtained from Youxuan Technology Corp. (Liaoning, China). All were used as obtained. The solutions used in this work were prepared with deionized water further purified with a Millipore Milli-Q (Millipore, Bedford, MA, USA) purification system (resistivity 18.6 MΩ).

3.2. The Preparation of TiO_2 Film Photoelectrodes and TiO_2 Powder

In this step, 15 mL ethanol containing 0.3 mL water was added dropwise into the mixture of 5 mL tetrabutyl titanate, 30 mL ethanol, and 0.3 mL nitric acid, stirring vigorously. Then, the whole mixture was continuously stirred for 2 h. A colorless and transparent TiO_2gel was obtained by keeping the whole mixture sealed for one day. On an FTO glass substrate (1.5 × 2.5 cm^2), a thin film of sol was spin-coated at 2000 rpm for 30 s, followed by annealing in air with different ramping rates to the final 500 °C. FTO substrates with 1, 2, 4, 8, 16, 20, 24, 32 layers of coatings were achieved by repeating the spin-coating process and were denoted as TiO_2-1, -2, -4, -8, -16, -20, -24, and -32, respectively. TiO_2 electrodes with 1 × 1 cm^2 of surface exposed were prepared by sealing them with epoxy resin. TiO_2-20 was chosen for XRD measurement. TiO_2 powder was collected by scraping the films off several TiO_2-20 samples.

3.3. Characterization of TiO_2 Films

XRD measurements were carried out on a PW 1840 powder X-ray diffractometer, using Cu Ka (1.54 Å) as the incident radiation. SEM images were obtained on a field-emission scanning electron microscopy (JSM-6700F, JEOL, Tokyo, Japan) at 30 kV. TEM were carried out with JEOL JEM100CXII. The absorption spectra were measured by a UV–vis spectrophotometer (CARY5000, Varian, Australia). The thickness of films was determined by a step profiler (Dektak XT, Bruker, Germany). Photoelectrochemical measurements and characterizations were conducted by a three-electrode system with a TiO_2 film electrode as working electrode, Pt plate electrode as counter electrode, and Ag/AgCl electrode as reference electrode, respectively, on a CHI660D station (Chenhua, Shanghai, China). The electrolytes were either 0.5×10^{-3} M $K_4Fe(CN)_6$ + 0.5×10^{-3} M $K_3Fe(CN)_6$ or air-saturated 1.0×10^{-3} M Na_2SO_4 solution. The light source was a UV-LED whose spectrum was given in Figure S1. The light intensity was measured by a light meter (LI-COR, Lincoln, NE, USA), and the light intensity for the experiments was fixed at 100 mW/cm^2.

3.4. Detection of •OH,•O_2^- and H_2O_2

The production of •OH was detected by a photoluminescence (PL) method by using terephthalic acid (TA) as a probe molecule [49]. The experimental procedure was similar to the measurement of PEC and PC activity except that the MO aqueous solution was replaced by the 5×10^{-4} M TA aqueous solution with a concentration of 2×10^{-3} M NaOH. The superoxide radical (•O_2^- was measured by XTT [50,51], which can be reduced by •O_2^- to form XTT-formazan. The formazan has an absorption spectrum (measured by UV/Vis spectrophotometer (Blue Star A, Fort Lauderdale, FL, USA) with a peak at 470 nm can be used to quantify the relative amount of superoxide. H_2O_2 was analyzed photometrically by the Peroxidase (POD)-catalyzed oxidation product of DPD [52,53], which was measured by UV/Vis spectrophotometer (CARY5000, Varian, Australia) at 551 nm.

3.5. PC and PEC Experiments of TiO_2 Photoelectrodes

Scheme 1 shows four kinds of reactors: (a) PEC reactor, in which TiO_2 film, Pt were used as working electrode, counter electrode, respectively; (b) PC reactor, in which TiO_2 film was dipped in solution; (c) membrane-separated (MS) reactor, and (d) PEC membrane-separated (PECMS) reactors which are the same as (a), (b), respectively, except that the reactors are separated into two compartments by a semipermeable membrane. The photographs of experimental set-up of PEC, PC reactors and MS, PECMS reactors are given in Figure S2. The pore size of the semipermeable membrane was 5 nm, whereas that of MO was about 6–8 nm in size so that MO cannot pass through the membrane. PEC degradation of MO was conducted with the TiO_2film as working electrode, Pt wire electrode as counter electrode, respectively, on a DXW-12V100A DC Voltage Regulator (Suzhou, China). At different time intervals, aliquots of the sample were collected. The MO concentration was analyzed by recording variations in the absorption band maximum at 465 nm (defined as A_t) in the UV-vis spectra of MO by using a UV-vis spectrophotometer. MO concentration of the reaction solution was defined as $A_{0'}$. The degradation efficiency of MO was calculated according to the equation: degradation rate (%) = $(A_{0'} - A_t)/A_{0'} \times 100\%$. The liquid phase degradation of MO was used for the evaluation of the PC activity of the TiO_2 powder.

4. Conclusions

The effects of bias, film thickness, pH value, and ion properties on the PEC performance of TiO_2 films were systematically studied under UV irradiation. At an optimized bias of 1.0 V, the TiO_2-20 photoelectrode can degrade 84.5% of MO in 6 h, which outperforms the other TiO_2 film samples. We observed that a high pH value contributed to enhanced degradation of MO. The "activated" halide ions can significantly promote PEC efficiency and the order of PEC efficiency was determined as Br > Cl > F. The degradation rate increased with an increasing Cl content in an MO solution, up until the optimized value of 30×10^{-3} M. However, excessive Cl content causes a decrease in degradation rate. The PEC efficiency can be significantly improved and a complete degradation of MO was achieved in 1.5 h using TiO_2-20 with 1.0 V bias and 30×10^{-3} M Cl ion content at Ph 12. The roles of ROSs and electric charge of electrodes were investigated to explore the related PEC mechanisms and H_2O_2, •O_2^-, and •OH were found responsible for the decolorization of MO.

Supplementary Materials: The following supporting information can be downloaded at: https://www.mdpi.com/article/10.3390/molecules28247967/s1, Figures S1–S4. Figure S1: The light spectrum of the UV lamp used in irradiation experiments. The peak is located at 365 nm. Figure S2: The photographs of experimental set-up of (a) PC, PEC reactors and (b) MS, PECMS reactors. Figure S3: The short circuit photocurrent (a), open circuit potential (b) and (c) absorbance of TiO_2-1, -2,-4, -8, -16, -20, -24 and -32. (d) variation of film thickness as the layers of coatings. Figure S4: PEC degradation of MO byTiO_2-1, -8, -16,-20 and 32 photoelectrodes at 1.0 V bias under UV irradiation.

Author Contributions: Conceptualization, J.L. and G.W.; methodology and data analysis, Y.X. and S.M.; writing—original draft preparation, Y.X. and S.M.; writing—review and editing, X.H.; super-

vision and funding acquisition, J.L. and G.W. All authors have read and agreed to the published version of the manuscript.

Funding: This research received no external funding.

Institutional Review Board Statement: Not applicable.

Informed Consent Statement: Not applicable.

Data Availability Statement: Data are contained within the article and Supplementary Materials.

Conflicts of Interest: The authors declare no conflict of interest.

References

1. Pereira, J.C. Environmental issues and international relations, a new global (dis)orderthe role of International Relations in promoting a concerted international system. *Rev. Bras. Política Int.* **2015**, *58*, 191–209. [CrossRef]
2. Yahya, R.; Shah, A.; Kokab, T.; Ullah, N.; Hakeem, M.K.; Hayat, M.; Haleem, A.; Shah, I. Electrochemical Sensor for Detection and Degradation Studies of Ethyl Violet Dye. *ACS Omega* **2022**, *7*, 34154–34165. [CrossRef] [PubMed]
3. Hayat, M.; Shah, A.; Hakeem, M.K.; Irfan, M.; Haleem, A.; Khan, S.B.; Shah, I. A designed miniature sensor for the trace level detection and degradation studies of the toxic dye Rhodamine B. *RSC Adv.* **2022**, *12*, 15658–15669. [CrossRef] [PubMed]
4. Fujishima, A.; Honda, K. Electrochemical photolysis of water at a semiconductor electrode. *Nature* **1972**, *238*, 37–38. [CrossRef] [PubMed]
5. Carey, J.H.; Lawrence, J.; Tosine, H.M. Photodechlorination of PCB's in the presence of titanium dioxide in aqueous suspensions. *Bull. Environ. Contam. Toxicol.* **1976**, *16*, 697–701. [CrossRef] [PubMed]
6. Pruden, A.L.; Ollis, D.F. Photoassisted heterogeneous catalysis: The degradation of trichloroethylene in water. *J. Catal.* **1983**, *82*, 404–417. [CrossRef]
7. Tanaka, K.; Kato, H.; Kikuchi, T.; Yagishita, A. High flux VUV beamline for photochemical processing study at Photon Factory (abstract). *Rev. Sci. Instrum.* **1989**, *60*, 2252. [CrossRef]
8. Gerischer, H.; Heller, A. Photocatalytic Oxidation of Organic Molecules at TiO_2 Particles by Sunlight in Aerated Water. *J. Electrochem. Soc.* **1992**, *139*, 113–118. [CrossRef]
9. Nosaka, Y. Water Photo-Oxidation over TiO_2-History and Reaction Mechanism. *Catalysts* **2022**, *12*, 1557. [CrossRef]
10. Alaydaroos, A.H.; Sydorenko, J.; Palanisamy, S.; Chiesa, M.; Al Hajri, E. Efficient photoelectrocatalytic degradation of amoxicillin using nano-TiO_2 photoanode thin films: A comparative study with photocatalytic and electrocatalytic methods. *Chemosphere* **2023**, *339*, 139629. [CrossRef]
11. Zhang, Y.; Xiong, X.; Han, Y.; Zhang, X.; Shen, F.; Deng, S.; Xiao, H.; Yang, X.; Yang, G.; Peng, H. Photoelectrocatalytic degradation of recalcitrant organic pollutants using TiO_2 film electrodes: An overview. *Chemosphere* **2012**, *88*, 145–154. [CrossRef] [PubMed]
12. Zhang, H.; Wang, Y.; Liu, P.; Han, Y.; Yao, X.; Zou, J.; Cheng, H.; Zhao, H. Anatase TiO_2 crystal facet growth: Mechanistic role of hydrofluoric acid and photoelectrocatalytic activity. *ACS Appl. Mater. Interfaces* **2011**, *3*, 2472–2478. [CrossRef] [PubMed]
13. Wang, N.; Li, X.; Wang, Y.; Quan, X.; Chen, G. Evaluation of bias potential enhanced photocatalytic degradation of 4-chlorophenol with TiO_2 nanotube fabricated by anodic oxidation method. *Chem. Eng. J.* **2009**, *146*, 30–35. [CrossRef]
14. Li, L.; Jiang, L.; Yang, L.; Li, J.; Lu, N.; Qu, J. Optimization of Degradation Kinetics towards O-CP in $H_3PW_{12}O_{40}/TiO_2$ Photoelectrocatalytic System. *Sustainability* **2019**, *11*, 3551. [CrossRef]
15. Xiaoli, Y.; Huixiang, S.; Dahui, W. Photoelectrocatalytic degradation of phenol using a TiO_2/Ni thin-film electrode. *Korean J. Chem. Eng.* **2003**, *20*, 679–684. [CrossRef]
16. Selcuk, H.; Sene, J.J.; Anderson, M.A. Photoelectrocatalytichumic acid degradation kinetics and effect of pH, applied potential and inorganic ions. *J. Chem. Technol. Biotechnol.* **2003**, *78*, 979–984. [CrossRef]
17. Li, Z.; Luo, L.; Li, M.; Chen, W.; Liu, Y.; Yang, J.; Xu, S.M.; Zhou, H.; Ma, L.; Xu, M.; et al. Photoelectrocatalytic C-H halogenation over an oxygen vacancy-rich TiO_2 photoanode. *Nat. Commun.* **2021**, *12*, 6698. [CrossRef] [PubMed]
18. Farooq, U.; Ahmad, T.; Naaz, F.; Islam, S.U. Review on Metals and Metal Oxides in Sustainable Energy Production: Progress and Perspectives. *Energy Fuels* **2023**, *37*, 1577–1632. [CrossRef]
19. Pattnaik, A.; Sahu, J.N.; Poonia, A.K.; Ghosh, P. Current perspective of nano-engineered metal oxide based photocatalysts in advanced oxidation processes for degradation of organic pollutants in wastewater. *Chem. Eng. Res. Des.* **2023**, *190*, 667–686. [CrossRef]
20. Ge, S.; Sang, D.; Zou, L.; Yao, Y.; Zhou, C.; Fu, H.; Xi, H.; Fan, J.; Meng, L.; Wang, C. A Review on the Progress of Optoelectronic Devices Based on TiO_2 Thin Films and Nanomaterials. *Nanomaterials* **2023**, *13*, 1141. [CrossRef]
21. Jiao, M.; Zhao, X.; He, X.; Wang, G.; Zhang, W.; Rong, Q.; Nguyen, D. High-Performance MEMS Oxygen Sensors Based on Au/TiO_2 Films. *Chemosensors* **2023**, *11*, 476. [CrossRef]
22. Kavan, L.; Tétreault, N.; Moehl, T.; Grätzel, M. Electrochemical Characterization of TiO_2 Blocking Layers for Dye-Sensitized Solar Cells. *J. Phys. Chem. C* **2014**, *118*, 16408–16418. [CrossRef]
23. Hitchman, M.L.; Tian, F. Studies of TiO_2 thin films prepared by chemical vapour deposition for photocatalytic and photoelectrocatalytic degradation of 4-chlorophenol. *J. Electroanal. Chem.* **2002**, *538–539*, 165–172. [CrossRef]

24. Rodríguez-Pérez, M.; Rodríguez-Gutiérrez, I.; Vega-Poot, A.; García-Rodríguez, R.; Rodríguez-Gattorno, G.; Oskam, G. Charge transfer and recombination kinetics at WO3 for photoelectrochemical water oxidation. *Electrochim. Acta* **2017**, *258*, 900–908. [CrossRef]
25. Todinova, A.; Idigoras, J.; Salado, M.; Kazim, S.; Anta, J.A. Universal Features of Electron Dynamics in Solar Cells with TiO_2 Contact: From Dye Solar Cells to Perovskite Solar Cells. *J. Phys. Chem. Lett.* **2015**, *6*, 3923–3930. [CrossRef] [PubMed]
26. Gomes, W.P.; Vanmaekelbergh, D. Impedance spectroscopy at semiconductor electrodes: Review and recent developments. *Electrochim. Acta* **1996**, *41*, 967–973. [CrossRef]
27. Song, X.M.; Wu, J.M.; Yan, M. Photocatalytic and photoelectrocatalytic degradation of aqueous Rhodamine B by low-temperature deposited anatase thin films. *Mater. Chem. Phys.* **2008**, *112*, 510–515. [CrossRef]
28. Zanoni, M.V.B.; Sene, J.J.; Anderson, M.A. Photoelectrocatalytic degradation of Remazol Brilliant Orange 3R on titanium dioxide thin-film electrodes. *J. Photochem. Photobiol. A Chem.* **2003**, *157*, 55–63. [CrossRef]
29. Brugnera, M.F.; Rajeshwar, K.; Cardoso, J.C.; Zanoni, M.V. Bisphenol A removal from wastewater using self-organized TiO_2 nanotubular array electrodes. *Chemosphere* **2010**, *78*, 569–575. [CrossRef]
30. Selcuk, H.; Sene, J.J.; Zanoni, M.V.; Sarikaya, H.Z.; Anderson, M.A. Behavior of bromide in the photoelectrocatalytic process and bromine generation using nanoporous titanium dioxide thin-film electrodes. *Chemosphere* **2004**, *54*, 969–974. [CrossRef]
31. De Santana, H.; Temperini, M.L.A. Spectroelectrochemical study of iodide, iodate and periodate on a silver electrode in alkaline aqueous solution. *J. Chem. Interfacial Electrochem.* **1991**, *316*, 93–105. [CrossRef]
32. Liu, H.; Cao, X.; Liu, G.; Wang, Y.; Zhang, N.; Li, T.; Tough, R. Photoelectrocatalytic degradation of triclosan on TiO_2 nanotube arrays and toxicity change. *Chemosphere* **2013**, *93*, 160–165. [CrossRef] [PubMed]
33. Daghrir, R.; Drogui, P.; Ka, I.; El Khakani, M.A. Photoelectrocatalytic degradation of chlortetracycline using Ti/TiO_2 nanostructured electrodes deposited by means of a Pulsed Laser Deposition process. *J. Hazard. Mater.* **2012**, *199–200*, 15–24. [CrossRef] [PubMed]
34. Zhang, Q.; Fu, Y.; Wu, Y.; Zhang, Y.-N.; Zuo, T. Low-Cost Y-Doped TiO_2 Nanosheets Film with Highly Reactive {001} Facets from CRT Waste and Enhanced Photocatalytic Removal of Cr(VI) and Methyl Orange. *ACS Sustain. Chem. Eng.* **2016**, *4*, 1794–1803. [CrossRef]
35. Bai, J.; Liu, Y.; Li, J.; Zhou, B.; Zheng, Q.; Cai, W. A novel thin-layer photoelectrocatalytic (PEC) reactor with double-faced titania nanotube arrays electrode for effective degradation of tetracycline. *Appl. Catal. B Environ.* **2010**, *98*, 154–160. [CrossRef]
36. Wu, L.; Li, F.; Xu, Y.; Zhang, J.W.; Zhang, D.; Li, G.; Li, H. Plasmon-induced photoelectrocatalytic activity of Au nanoparticles enhanced TiO_2 nanotube arrays electrodes for environmental remediation. *Appl. Catal. B Environ.* **2015**, *164*, 217–224. [CrossRef]
37. Conway, B.E. Advancer in Electrochemistry and Electrochemical Engineering. In *Electrochemistry*; Delahay, P., Ed.; Interscience Publishers, Inc.: Hoboken, NJ, USA, 1961.
38. El Guibaly, F.; Colbow, K. Theory of photocurrent in semiconductor-electrolyte junction solar cells. *J. Appl. Phys.* **1982**, *53*, 1737–1740. [CrossRef]
39. Khan, S.U.; Bockris, J.O.M. A Model for Electron Transfer at the Illuminated p-Type Semiconductor-Solution Interface. *J. Phys. Chem.* **1984**, *88*, 2504–2515. [CrossRef]
40. Chandra, S.; Singh, S.L.; Khare, N. A theoretical model of a photoelectrochemical solar cell. *J. Appl. Phys.* **1986**, *59*, 1570–1577. [CrossRef]
41. Hodes, G.; Howell, I.D.J.; Peter, L.M. Nanocrystalline Photoelectrochemical Cells A New Concept In Photovoltaic Cells. *J. Electrochem. Soc.* **1992**, *139*, 3136–3140. [CrossRef]
42. Kambili, A.; Walker, A.B.; Qiu, F.L.; Fisher, A.C.; Savin, A.D.; Peter, L.M. Electron transport in the dye sensitized nanocrystalline cell. *Phys. E Low-Dimens. Syst. Nanostruct.* **2002**, *14*, 203–209. [CrossRef]
43. Guo, Q.; Zhou, C.; Ma, Z.; Yang, X. Fundamentals of TiO_2 Photocatalysis: Concepts, Mechanisms, and Challenges. *Adv. Mater.* **2019**, *31*, e1901997. [CrossRef] [PubMed]
44. Liu, F.; Cao, H.; Xu, L.; Fu, H.; Sun, S.; Xiao, Z.; Sun, C.; Long, X.; Xia, Y.; Wang, S. Design and preparation of highly active TiO_2 photocatalysts by modulating their band structure. *J. Colloid Interface Sci.* **2023**, *629*, 336–344. [CrossRef] [PubMed]
45. Schneider, J.; Matsuoka, M.; Takeuchi, M.; Zhang, J.; Horiuchi, Y.; Anpo, M.; Bahnemann, D.W. Understanding TiO_2 photocatalysis: Mechanisms and materials. *Chem. Rev.* **2014**, *114*, 9919–9986. [CrossRef] [PubMed]
46. Rincon, A. Effect of pH, inorganic ions, organic matter and H_2O_2 on *E. coli* K12 photocatalytic inactivation by TiO_2 Implications in solar water disinfection. *Appl. Catal. B Environ.* **2004**, *51*, 283–302. [CrossRef]
47. Fox, M.A. Photoinduced Electron Transfer in Organic Systems: Control of Back Electron Transfer. In *Advances in Photochemistry*; Volman, D.H., Hammond, G.S., Gollnick, K., Eds.; John Wiley & Sons, Inc.: Hoboken, NJ, USA, 1986; Volume 13, pp. 238–305.
48. Hu, Z.; Lyu, J.; Ge, M. Role of reactive oxygen species in the photocatalytic degradation of methyl orange and tetracycline by Ag_3PO_4 polyhedron modified with g-C_3N_4. *Mater. Sci. Semicond. Process.* **2020**, *105*, 104731. [CrossRef]
49. Ishibashi, K.I.; Fujishima, A.; Watanabe, T.; Hashimoto, K. Quantum yields of active oxidative species formed on TiO_2 photocatalyst. *J. Photochem. Photobiol. A Chem.* **2000**, *134*, 139–142. [CrossRef]
50. Sutherland, M.W.; Learmonth, B.A. The Tetrazolium Dyes MTS and XTT Provide New Quantitative Assays for Superoxide and Superoxide Disrnutase. *Free. Radic. Res.* **1997**, *27*, 283–289. [CrossRef]
51. Li, Y.; Zhang, W.; Niu, J.; Chen, Y. Mechanism of Photogenerated Reactive Oxygen Species and Correlation with the Antibacterial Properties of Engineered Metal-Oxide Nanoparticles. *ACS Nano* **2012**, *6*, 5164–5173. [CrossRef]

52. Bader, H.; Sturzenegger, V.; Hoigné, J. Photometric method for the determination of low concentrations of hydrogen peroxide by the peroxidase catalyzed oxidation of N,N-diethyl-p-phenylenediamine (DPD). *Water Res.* **1988**, *22*, 1109–1115. [CrossRef]
53. Wang, W.; Yu, Y.; An, T.; Li, G.; Yip, H.Y.; Yu, J.C.; Wong, P.K. Visible-light-driven photocatalytic inactivation of *E. coli* K-12 by bismuth vanadate nanotubes: Bactericidal performance and mechanism. *Environ. Sci. Technol.* **2012**, *46*, 4599–4606. [CrossRef]